Appl. Magn. Reson. 29, 65–88 (2005)

Applied Magnetic Resonance

Direct Detection of Neuronal Activity with MRI: Fantasy, Possibility, or Reality?

P. A. Bandettini[1,2], N. Petridou[1], and J. Bodurka[2]

[1] Unit on Functional Imaging Methods, Laboratory of Brain and Cognition and
[2] Functional MRI Facility, National Institute of Mental Health, National Institutes of Health, Bethesda, Maryland, USA

Received November 29, 2004; revised January 7, 2005

Abstract. Hemodynamic-based functional magnetic resonance imaging (fMRI) techniques have proven to be extremely robust and sensitive methods for noninvasive detection and mapping of human brain activation. Nevertheless, limitations in temporal and spatial resolution as well as interpretation remain because hemodynamic changes accompanying brain activation are relatively sluggish and variable and therefore imprecise measures of neuronal activity. A hope among brain imagers would be to possess a technique that would allow direct mapping of brain activity with spatial resolution on the order of a cortical column and temporal resolution on the order of an action potential or at least a postsynaptic potential. Recent efforts in understanding the direct effects of neuronal activity on MRI signal have provided some degree of hope for those who want a more precise noninvasive brain activation mapping technique than fMRI as we know it now. While the manner in which electrical currents influence MRI signal is well understood, the manner in which neuronal firing spatially and temporally integrates on the spatial scale of an MRI voxel to produce a magnetic field shift and subsequently an NMR phase and/or magnitude change is not well understood. It is also not established that this field shift would be large or long enough in duration to be detected. The objective of this paper is to provide a perspective of the work that has been performed towards the direction of achieving direct neuronal current imaging with MRI. A specific goal is to further clarify what is understood about the theoretical and practical possibilities of neuronal current imaging. Specifically discussed are modeling efforts, phantom studies, in vitro studies, and human studies.

1 Introduction

The type of questions that researchers can ask regarding the functional organization of the human brain are tightly intertwined with the technology and methods at their disposal. In the past decade, the development of functional magnetic resonance imaging (fMRI) has precipitated an explosion of effort and new findings because of its ease of implementation, temporal and spatial resolution, and sensitivity. While applications for and sophistication of fMRI continues to grow, researchers are daily confronted with its limitations in temporal and spatial resolu-

tion, sensitivity, and interpretability [1, 2]. These limitations are inherent to the hemodynamic origin of the functional contrast.

Most applications of fMRI use blood-oxygenation-level-dependent (BOLD) contrast [3]. The basis of BOLD contrast is the oxygen-dependent magnetic susceptibility of hemoglobin. Deoxyhemoglobin is paramagnetic relative to tissue. This difference in susceptibility creates magnetic field distortions which lead to dephasing. During brain activation, localized increases in blood flow increase blood oxygenation and consequently reduce deoxyhemoglobin, causing the MRI signal to increase. This signal begins to increase approximately 2 s after neuronal activity begins and plateaus in the "on" state after about 7 to 10 s. The dynamics, location, and magnitude of the signal is highly influenced by the vasculature in each voxel [4]. If voxels happen to capture large vessel effects, the magnitude of the signal may be large (up to an order of magnitude larger than capillary effects), the timing a bit more delayed than average (up to 4 s delayed from capillary effects), and the location of the signal somewhat distal (up to a centimeter) from the true region of activation. While significant improvements are being made in fMRI methodology such that these variables are kept to a minimum, they nevertheless remain at all field strengths and limit the depth and range of questions that can be addressed by fMRI.

The emergence of a technique that is able to more directly map neuronal activity at the spatial and temporal resolution with which it takes place would certainly lead to another acceleration of insights into human brain functional organization and clinical applications. Before hemodynamic contrast for fMRI was discovered, physicists have considered the sensitivity of MRI signal intensity to neuronal activity. Anecdotally, at least a handful of physicists have mentioned that either experiments were attempted or calculations performed at some point even as far back as 15 years ago to determine the possibility of using MRI to directly detect neuronal activity. The experiments were all either negative or inconclusive and the calculations typically yielded theoretical effects that were several orders of magnitude below the detection threshold of the time. In recent years, with the success of fMRI, physicists have begun rethinking the possibility of using MRI to directly detect neuronal activity. MRI sensitivity and imaging techniques have substantially improved, the dynamics of neuronal activation are better understood, and experimental techniques have improved.

In this paper, the progress in neuronal current MRI, here termed ncMRI, is traced historically. Techniques, results, and models are critically summarized and compared in depth. Lastly, a detailed discussion of the current limits, potential solutions, and the ultimate feasibility of fMRI is provided.

2 Neuronal Current Imaging

An initial understanding of ncMRI can be obtained by an analogy to BOLD contrast. For clarity in this paper, neuronal current-dependent contrast will be termed CURD. The similarities of BOLD and CURD contrast are that both are

fundamentally highly localized alterations in the main magnetic field of the scanner which, depending on the geometry (size, shape, distribution, and orientation) of the source (vasculature or neuronal bundle), cause a phase shift and/or magnitude change. Single orientation, large (comparable to a voxel size or larger) geometries (large vessels or simplified dipoles) cause phase shifts, while small, random geometries generally cause magnitude changes (phase dispersion modulation). The differences between BOLD and CURD are that, by most calculations [5, 6], but not all [7], the magnetic field related to CURD contrast is an order of magnitude less than that of BOLD contrast. The spatial distribution of the field distortion for a given geometry differs between the two contrasts. The magnetic field geometry around a current-carrying wire in a magnetic field (dipole) as with CURD, is different from the magnetic field around a wire in a magnetic field which has a different susceptibility to its surrounding environment (quadrupole) as with BOLD. The precise geometry of sources of CURD contrast is much less well understood than that with BOLD contrast. While the spatial scales and magnetic field effects of individual neurons and dendrite bundles are well understood [8], the spatial and temporal scales of how their activity is integrated to affect the magnetic field on larger spatial scales is not understood. The basics of neuronal activity are relevant to this article and are included as an appendix. In particular, the precise temporal synchrony across millimeters and centimeters is not understood. While hemodynamic effects are sluggish enough to integrate over the time course of seconds, neuronal current effects may take place in single neurons or across large areas of tissue, and their duration can be 1 to 400 ms. Not only is it difficult to predict exactly how their activity will spatially and temporally integrate, it is also a practical challenge (discussed later) to choose an MRI time window (typically about 30 ms for echo planar imaging [EPI]), with which to try to capture these transient effects.

Another important difference between CURD and BOLD contrast is that the field distortion magnitude for CURD contrast is not proportional to the main magnetic field as BOLD contrast is. CURD contrast is simply an additive effect onto the primary magnetic field, showing the same magnitude whether 0.5 or 7 T is used for imaging.

Lastly, other effects of CURD contrast may be manifest, such as Lorentz forces causing physical displacement of synchronously firing neuronal bundles [9]. The effects of Lorentz forces (small displacements) may be amplified by additional diffusion weighting. While not a neuronal current effect in itself, changes in apparent diffusion coefficient [10, 11] and T_1 (or M_0) [12, 13] have been observed to correspond to neuronal activity and not hemodynamic effects. The hypothesized physiologic mechanism for this effect has been cell swelling with increased activity. An alternative explanation for these observed changes in diffusion coefficient is a cooling of the brain by the increase in cerebral blood flow [14, 15].

Because of the difficulty to precisely model CURD contrast, it is extremely challenging to predict experimental failure or success. In the face of this uncertainty, many groups have forged ahead and carried out experiments ranging from phantom studies to cell culture studies to human studies. Below is a criti-

cal overview of the approximate chronology of theoretical and experimental progress in ncMRI over the past 15 years. It is exciting to note that in recent years, these efforts have increased in parallel with improvements in sensitivity, resolution, experimental design, and processing.

2.1 Chronology of ncMRI

Among the first to demonstrate MRI of magnetic fields in biological tissue were Joy et al. [16] in 1989. In their study, current pulses of 2 mA lasting 40 ms were injected in the forearm of a human subject and MR images were acquired with standard multishot spin-echo data acquisition (repetition time [TR], 1 s; echo time [TE], 60 ms; slice thickness, 2 cm). Phase images obtained with this technique clearly demonstrated localized magnetic field changes associated with the applied current. Phantom experiments were also performed in this study with a similar spin-echo acquisition that allowed detection of phase shifts induced by current pulses injected in electrodes immersed in saline (current pulse, 43 mA; duration, 50 ms). Even though this work demonstrated that MRI could be used to directly detect local MR phase shifts induced by biological magnetic fields, it was based on applied currents, as opposed to intrinsic electrical activity. Furthermore, the applied currents were several orders of magnitude higher than currents expected from neuronal activity. This same group expanded on this current density imaging technique to include imaging of radio-frecuency (RF) current density in biological tissue [17]. One potential application was to map in three dimensions electrical conductivity heterogeneity in biological tissue.

The first published attempt to detect intrinsic neuronal magnetic fields with MRI was by Singh [18] in 1994. The study was performed at 1.5 T and used a standard multishot spin-echo imaging technique (TR, 2 s; TE, 100 ms) to detect phase shifts induced by neuronal activation in human subjects during auditory stimulation (1 kHz tone, 400 ms on and 1600 ms off, delay between stimulus onset and 90° pulse varied from 75 to 200 ms). Although the findings of this study were negative, as sensitivity of the MRI system and imaging technique was a factor of 20 lower than that required to detect neuronal magnetic fields, according to the calculations in the paper, the approach was innovative. The use of a spin-echo pulse sequence was explicitly to "tune" the acquisition to transient shifts in B_0 which then reverse polarity. The oppositely polarized currents would induce a net MRI phase shift of zero for a gradient-echo sequence at a similar TE but a maximal phase shift for a spin-echo sequence since the phase accumulation is reversed at TE/2 by the 180° pulse. The timing of neuronal activation was determined in the same study by the use of a superconducting quantum interference device (SQUID) neuromagnetometer. Although this is a good first estimate of neuronal activity timing, it is not established that neuronal dynamics as they are detected at the surface of the skull are the same as those to be measured in a voxel. It is possible that highly variable dynamics spatially and temporally sum to create the waveform that is measured by a

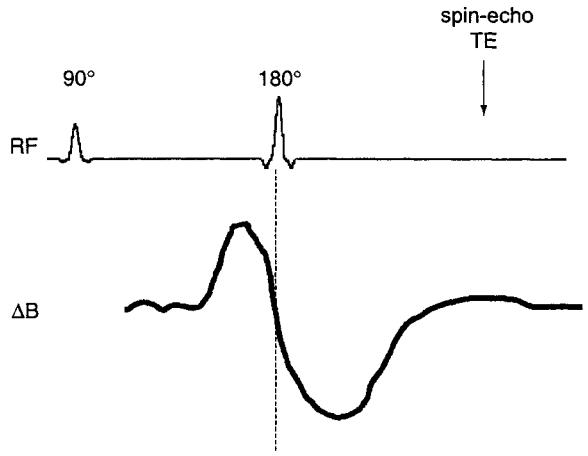

Fig. 1. Illustration of a spin-echo pulse sequence, which is optimally "tuned" to detection of transient and bipolar changes in magnetic field induced by brain activation. The bottom curve shows the hypothesized change in magnetic field with brain activation (as typically measured with MEG). It is typically manifest as an increase (or decrease) in magnetic field, then a decrease (or increase) in magnetic field. The entire waveform is played out in approximately 100 to 300 ms. An ideal spin-echo timing is shown here. The 180° pulse is applied as the magnetic field reverses polarity. Without the 180° pulse (a gradient-echo sequence), the phase accumulation (integral under the ΔB curve) would be approximately zero, but with the 180°, the ΔB curve is rectified, leading to a maximal phase accumulation.

SQUID magnetometer, which, in turn, may not resemble the individual waveforms at the smaller spatial scale. A diagram of the hypothetical experiment is shown in Fig. 1.

The study by Singh [18] is significant. It was the first to estimate the minimal phase shift detectability with the achievable signal-to-noise ratio (SNR) at the time (about 6 degrees). It was the first to use a current phantom to simulate neuronal activity. It was the first to use human SQUID measurements to estimate the degree of neuronal activation and the relative timing. A prescient quote in the paper, in the face of a factor of 20 difference in required sensitivity, and one that is all the more relevant today is: "Nonetheless, human studies were conducted in the hope that local current densities in cortical regions, which produce the phase shifts in the MRI studies, might be much larger than the aggregate current densities producing the external magnetic field." As mentioned, we still do not know the precise manner in which neuronal currents add up in the brain to produce the magnetic field fluctuations that are detected at the surface. It is indeed possible that significant current polarity cancellation is taking place at a spatial scale of MRI, producing a set of greater magnetic fields at the "dipole" sources than those predicted by a simple model which takes into consideration a 100 fT field at the surface of the scull and a radius cubed or radius squared falloff in magnetic field from the source which is several centimeters away.

In 1999, a study by Bodurka et al. [19] was among the first to use EPI time series data to assess the effects of injected current on MR phase and magnitude

around the current-carrying wire. The phantom used in the study consisted of a copper wire (diameter, 60 μm) immersed in a water solution. Current pulses ranging from 10 to 100 μA in a cycle of 2 s on and 2 s off were used. MR images were obtained with a gradient-echo EPI typically used for BOLD imaging, however at a higher sampling rate and higher resolution (TR, 54 or 100 ms; TE, 27.2 ms; field of view [FOV], 12 cm; imaging matrix, 64 by 64 pixels; slice thickness, 7 mm). Results from this study demonstrated detection and mapping of phase shifts on the order of 0.8±0.1 degrees (1.7±0.3 nT magnetic field change), induced by a 10 μA electric current pulse.

An interesting yet potentially misleading finding from this report is that because a current through a single wire produced the simulated dipole source, and because the spatial distribution of this magnetic field was on the order of a voxel size, MRI phase shifts were significantly larger than magnitude changes. This was particularly true if the wire were not centered in the imaging voxel. The symmetry of the magnetic field distribution around the wire causes phase cancellation, but if the wire is off center, this cancellation does not occur since the entire symmetrical phase distribution is not sampled within a single voxel. The reason why this effect is potentially misleading is that in cortex, a dipole likely consists of at least tens of thousands of dendrites that have a predominant net orientation but a distribution of orientation directions on a smaller spatial scale. While it is true that without coherence in orientation over some spatial scale in the brain, nothing would be detected at the surface of the skull, it is also true that around each dendrite bundle (millions within a voxel), phase coherence is being modulated. If the scale is large enough such that the microscopic field inhomogeneity effect is not completely washed out by spatial averaging from proton diffusion (a larger size than about 5 mm), a significant MR magnitude change (signal decrease) would also accompany an increase in neuronal activity. Therefore, both magnitude changes (small scale effect) and phase changes (large scale effect) would occur. This effect, while straightforward to simulate, is extremely difficult to model with a phantom. Phantom results, while giving first-order estimates of what neuronal "dipoles" resemble, are missing the finer spatial scale effect.

A second effort at imaging neuronal currents in humans was published by Kamei et al. [20] in 1999. The strategy presented is based on the idea that the manifestation of neuronal current effects is dependent in one direction on the gradient polarity, while susceptibility effects are not. Therefore, two manipulations are performed: rest and active, positive and negative gradient polarity. If the rest minus active images for both the positive and negative polarity are subtracted from each other, then susceptibility effects are subtracted out, while neuronal current effects, theoretically, are not. The authors claim to successfully produce images of activation-induced neuronal current distribution. The reproducibility of these results remains to be demonstrated. Other recent work on modeling of neuronal current effects and determining the lower detectability limit for ncMRI has been published by this group [21]. Their calculations determined a lower theoretically detectable limit of $1.68 \cdot 10^{-9}$ T and a practical limit (given scanner stability and signal-to-noise considerations) of a value that is 10 times

greater. Lastly, Sekino et al. [22] (also from this group) recently published a report demonstrating an RF pulse-based method for detecting transient neuronal currents.

In 2001, Song et al. [9] put forth a novel method for potentially detecting neuronal currents in larger (and clearly single-orientation) neuronal bundles. In this study, the Lorentz effect (spatial displacement due to the force acting on a conductor carrying electric currents and placed in the external MR magnetic field) was utilized to demonstrate that observation of the displacement of a wire containing current of a magnitude similar to that of nerve fibers is possible. The phantom used consisted of a standard copper wire immersed in a gel solution. Current pulses ranging from 100 to 500 μA were applied and spin-echo MR images were acquired at 7 T, demonstrating minute spatial displacements associated with the current pulse. The study suggested that Lorentz effect imaging could potentially be utilized to indirectly map axonal neuronal currents, i.e., currents in white matter as opposed to cortical activation.

Diffusion gradients may enhance sensitivity to Lorentz force displacement on conducting nerves. Such is a potential explanation provided by Song et al. [23] for preliminary results in which rapid brain activation-correlated signal decreases (an increase in diffusion coefficient) were observed with images obtained using extremely high diffusion weighting. A recent article by Yamaguchi et al. [24] demonstrated that the apparent diffusion coefficient of rat brain tissue increased when external electrical currents were applied. The mechanism that they put forth to explain this effect is an increase in ion movement in extracellular space in tissue, not necessarily associated with an increase in activation.

Several groups have observed brain activation-induced decreases in apparent diffusion coefficient [10, 11] which would produce activation-induced signal increases in diffusion-weighted sequences. One hypothesized mechanism for these changes is cell swelling with activation. While controversial, a simple explanation for cell swelling causing decreases in diffusion coefficient is that intracellular diffusion coefficient of protons is thought to be less than that of extracellular protons. A redistribution of protons to intracellular space would lower the average diffusion coefficient. In addition, the use of high b factors helped rule out hemodynamic contributions.

In 2002, Bodurka et al. [5] published a study that helped advance ncMRI along several avenues. It presented a straightforward yet novel calculation for the expected field change in a voxel that utilized information from magnetoencephalography (MEG) and information from neuroanatomy and electrophysiology. It addressed the issue of physiologic fluctuations and put them in the context of neuronal current detection. It further advanced the use of spin-echo rather than gradient-echo EPI with regard to enhancement of high-temporal-frequency neuronal current effects and attenuation of less-high-frequency (<10 Hz) artifactual phase shifts that can occur with respiration hemodynamic changes, and uncharacterized signal drift.

The calculation of the expected change in the magnetic field, B, was as follows: A single dendrite, having a diameter d, length L, current I, and voltage V,

behaves like a conductor with conductivity σ. Resistance is $R = V/I$, where $R = 4L/(\pi d^2\sigma)$. From Biot–Savart law: $B = (\mu_0/4\pi)((I/L)/r^2) = (\mu_0/16)(d^2\sigma V/r^2)$. By substituting $d = 4$ μm, $\sigma = 0.25\ \Omega^{-1}\text{m}^{-1}$, $V = 10$ mV, and $r = 4$ cm (typical distance from a dipole source and surface of the skull), the resulting value measured at the surface of the skull from a single dendrite is about 0.002 fT.

Given that the typical MEG measurement at the surface of the skull is on the order of 100 fT, then at least 50000 dendrite bundles ($0.002 \times 50000 = 100$ fT) must coherently act to generate such a field. These bundles of neurons produce, within a voxel that has dimensions of 1 mm^3, a field on the order: $B_{\text{mri}} = B_{\text{meg}}(r_{\text{meg}}/r_{\text{mri}})^2 = B_{\text{meg}}(4\ \text{cm}/0.1\ \text{cm})^2 = 1600B_{\text{meg}} = 0.2$ nT.

Assuming an r^2 drop-off of B_0 as a function of distance from the source (in fact, the relationship varies from r to r^3 depending on the precise geometry and

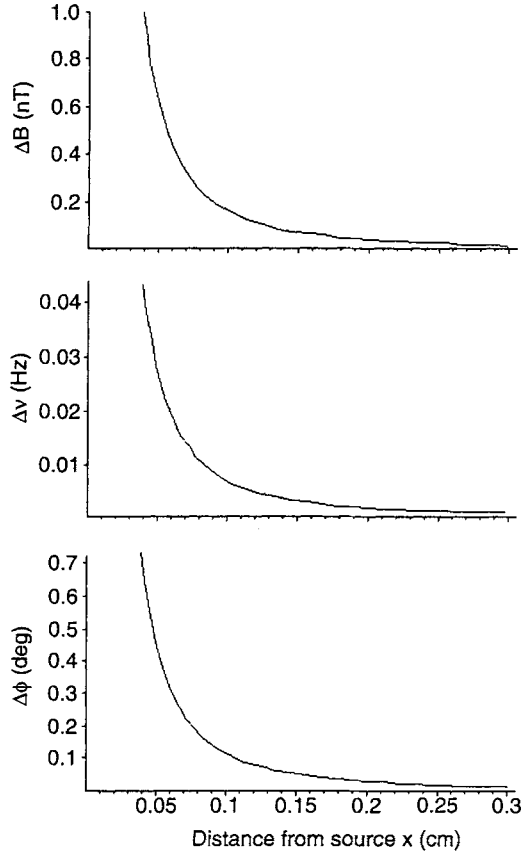

Fig. 2. With the use of a simplified dipole model for a current source producing 100 fT 4 cm away (skull surface), the plots show the magnetic field $\Delta B = 100\ \text{fT} \cdot (4\ \text{cm}/x)^2$ in nanotesla (top), frequency offset $\Delta\nu = \gamma \cdot \Delta B$ in hertz (middle), and subsequent phase shift $\Delta\phi = \Delta\nu \cdot \text{TE} \cdot (180/\pi)$ (bottom) as a function of distance from the source (in centimeters). This distance is from 0 to 0.3 cm (size of typical EPI voxel).

distance), the neuronal current-induced shift in B_0, frequency ν, and phase ϕ (assuming a gradient-echo time of 40 ms) are shown in Fig. 2. It is useful to note that extremely close to the dipole source, ΔB_0 becomes extremely high. Given the uncertainty of the dipole size and/or number and distribution of dipoles, it is possible that if a voxel size is chosen to minimize partial volume averaging, a relatively large phase shift would be observed.

So, the primary question posed in this paper by Bodurka et al. is whether or not a 0.2 nT (or about 0.01 Hz or 0.1° phase shift) B shift would be detectable. This is not only a function of image SNR but, more importantly, of physiologic noise and how well it can be removed or avoided. It is also dependent on how effectively a temporally and spatially variable cascade of transient neuronal activity can be captured with MRI, which has a rapid acquisition rate but with prohibitively large temporal gaps due to the limitations of TR.

In Bodurka et al. [5], time course fluctuations in phase were calculated to be on the order of 10 nT. It was also demonstrated that spin-echo sequences show a much smaller level of phase fluctuation. A simple Fourier transform of the phase time course revealed respiration as the source of these fluctuations, shown in Fig. 3. To further test this effect with a current phantom, an additional sinusoidal electric current was included in the already present neuronal current pulse. In ref. 5, a comparison between gradient-echo and spin-echo EPI was performed (TR, 1 s; TE, 30 ms for gradient-echo and 60 or 90 ms for spin-echo; FOV, 16 cm, imaging matrix, 64 by 64 pixels; slice thickness, 6 mm). The results from this study demonstrated that spin-echo EPI is more sensitive to weak

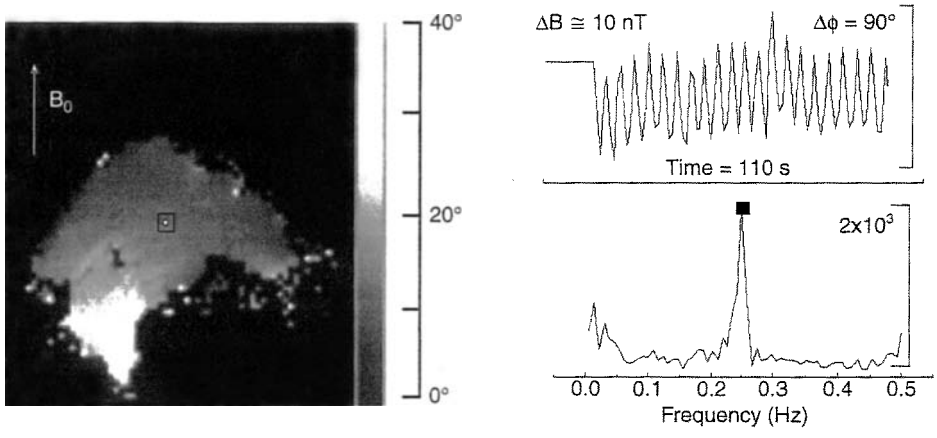

Fig. 3. Effect of respiratory motion on the signal phase as discussed in ref. 5. The image on the left shows a map of the phase shift at the respiration frequency obtained from a time series collection of phase images. The gray scale is in degrees. Note the spatial distribution of the phase effects. The time series signal (over 110 s) from the center voxel in the square box on the image is shown on the top right. The peak-to-peak variation is approximately 90°, corresponding to a magnetic field shift of 10 nT. This is at least an order of magnitude larger than the hypothesized neuronal current-induced phase shift. The plot on the bottom right shows the Fourier transform of the time series, demonstrating that it has the periodicity of respiration.

and transient magnetic field changes than gradient-echo EPI. Spin-echo EPI has the inherent characteristic of refocusing the phase accumulation associated with slowly changing phase that may originate from hardware instabilities or baseline physiology (such as respiration), which is of significance for in vivo applications. The spin-echo EPI method and MRI system used allowed for the detection of transient magnetic fields of 0.2 nT or 0.1° phase shift, lasting for 40 ms, which is on the order of magnetic fields produced by neuronal activation in cortex. This result is shown in Fig. 4. While the estimates for the magnitude of CURD con-

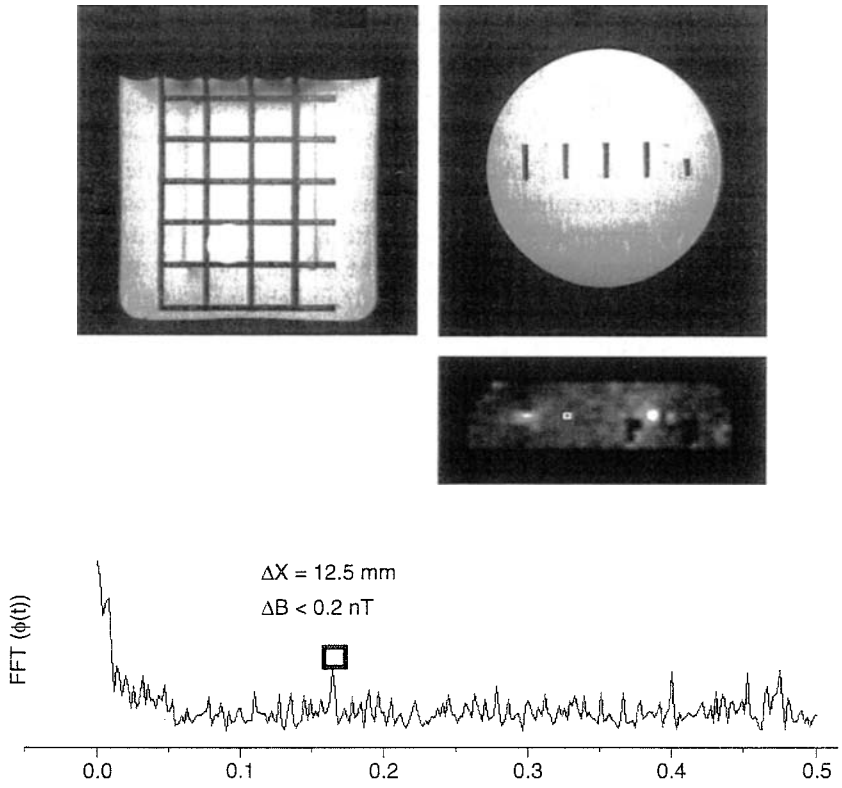

Fig. 4. Experimental setup and results to simulate the direct observation of neuronal currents [5]. The top two images are of the neuronal current phantom: a beaker of copper sulfate containing current-carrying wires having opposite polarity. In this experiment, the current in the wire was modulated both at the frequency of respiration and at a higher frequency simulating transient neuronal activity. The image below these two images is of the correlation of a model reference function (neuronal current effect) with the time series of the images. The acquisition was carried out using spin-echo EPI "tuned" to the timing of the transient (refer to Fig. 1) and designed to suppress slow, respiratory-like, changes. The plot on the bottom is of the Fourier transform on the time series from a voxel approximately 12.5 cm from the current source in the phantom (indicated by the box). It was calculated, on the basis of the wire geometry, that at 12.5 cm from the wire, transient magnetic field shift is 0.2 nT. This indicates not only that the respiration effects were mostly suppressed but that 0.2 nT is detectable.

trast and the detection limit are shown to be the same here, they are of course based on simplifying assumptions of neurophysiology and current-carrying geometry. Nevertheless, the results in this work indicate the first time in which estimates of minimum detection level and the magnitude of the effect were within the same order of magnitude – at least in phantom data simulating physiologic noise.

A more recent study by Konn et al. [6] provided a more complete theoretical and experimental validation of previous work. In ref. 6, a more realistic model and experimental phantom (true dipole rather than a wire) were used. The mathematical model was developed to examine the feasibility of ncMRI and predict the MR phase and magnitude changes induced by neuronal activation. Neuronal currents were modeled as extended current dipoles located in a homogeneous conducting sphere modeling the head. The magnetic field distribution within the sphere, close to, and inside the current dipole, was modeled, and contributions from both primary (propagation path) and volume (return path) currents were considered. Simulations suggested that a dipole of 4.5 nA could be detected with MRI, and, again, it was established that phase imaging allowed for the better sensitivity to current-induced MR signal changes than magnitude imaging. A further finding was that volume current contribution to the dipole-induced magnetic field is negligible in the vicinity of the current source and becomes significant near the surface of the sphere. Theoretical predictions were verified experimentally with a dipole phantom and gradient echo EPI imaging at 3 T (TE, 23–35 ms; TR, 45–1000 ms; FOV, 25.6 cm; imaging matrix, 64 by 64 pixels; slice thickness, 9 mm). In the experimental work, magnetic fields of 0.110 ± 0.050 nT were detected, associated with a dipole strength of 6.3 nA.

In 2003, a study was published by Xiong et al. [7] which claimed success in using MRI to directly map neuronal currents in humans. They coined the technique "magnetic source MRI" (msMRI). With a paradigm in which a subject was asked to execute a motor command on seeing a visual stimulus, they demonstrated a 1% magnitude change primarily in motor cortex that occurred, importantly, within 150 ms of the onset of the finger movement. The visual and motor task alternated with a period of rest (1 s on and 1 s off) and MR images were acquired at -200, -100, 0, 100, and 200 ms relative to the stimulus onset (visual cue). Subjects indicated the presence of a wedge of random dots in their lower left visual field by pressing and releasing a button with the index finger. MR images were acquired at 1.9 T with a gradient-echo EPI (TR, 1 s; TE, 100 ms; slice thickness, 6 mm; FOV, 20 cm). The experimental design was aimed to induce a steady saturated "on" state in the slower-responding BOLD contrast response. The effective sampling time of 100 ms was obtained by systematically shifting the onset of the task relative to the image acquisition. This general type of strategy is illustrated in Fig. 5, in which the arbitrarily long TR is chosen such that it is not an even multiple of the interstimulus interval (ISI). Here the ISI is 1 ± 0.1 and 0.2 s.

The primary finding of ref. 7 was that surprisingly large magnitude changes (1% signal decrease) and no phase changes were reported. Although a magnitude change

of 1% can be modeled with a high estimate (about double than that typically used) for neuronal packing density and a mesh of dendrites with sufficient spacing and appropriate randomness as well as the assumption of complete synchronicity, it is difficult to predict that only a magnitude change with no phase change would occur given the fact that there is a MEG measurable effect on a larger spatial scale (which must be manifest as a net phase shift at some spatial scale) – otherwise no net magnetic field would be detected at the surface of the skull. In general, the size of the effect reported is about an order of magnitude larger than that predicted by most models.

A schematic clarification for the phase versus magnitude effect controversy is provided in Figs. 6 and 7. Figure 6 shows the types of magnetic fields that are produced by a unit of neuronal activity. Here we assume that the cylinder conductor is a single dendrite or axon or a bundle of dendrites that have a net distribution perpendicular to the cortex. During an action potential, a rapid depolarization and slow repolarization of membrane potential occurs as ions travel across the membrane. This cross-membrane current produces a rapidly changing sink and source potential. The propagation of this potential is also manifest as an intracellular current that travels in the direction of the nerve orientation. As current propagates through the conductor a surface magnetic field is created. This surface magnetic field is shown schematically at the bottom of Fig. 6. If a group

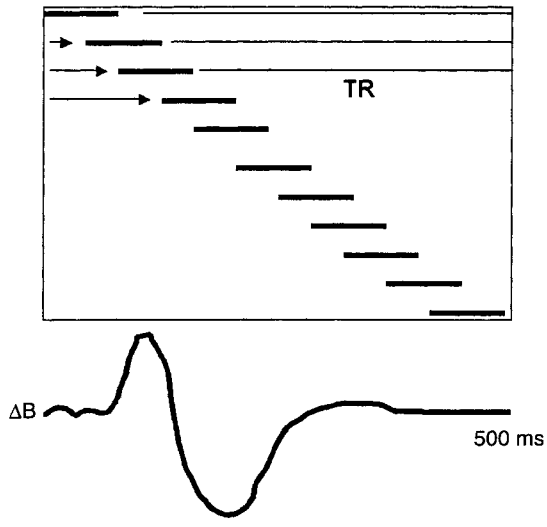

Fig. 5. Schematic illustration of a method to sample a neuronal current waveform used in ref. 7, shown at the bottom, at high temporal resolution. The thick lines at the top of the figure show the width of an EPI readout window (about 25–40 ms). The TR is arbitrarily long yet is such that the neuronal onset time is shifted every TR and repeats after a sufficient sampling is accomplished. In this manner, extremely high resolution sampling of the transient neuronally induced magnetic field changes, shown at the bottom, is achieved even with the limitation of a relatively long minimal TR when performing multislice EPI.

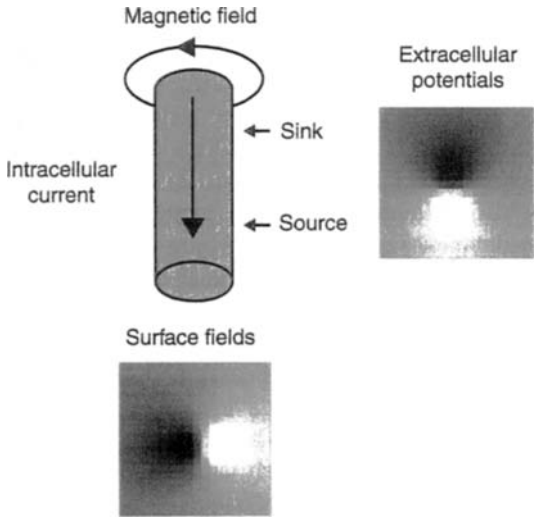

Fig. 6. Schematic illustration of the magnetic fields produced by neuronal activity. The diagram on the top left is a depiction of a simplified model of a dendrite. Highly transient and rapidly traveling extracellular fields are produced as intracellular and extracellular ion exchange occurs, producing highly transient (<10 ms) magnetic field changes having a spatial distribution pattern shown on the top right. An intracellular current also exists. This travels along the dendrite and produces a magnetic field (the surface field) around it with a spatial distribution shown at the bottom. The timing of these effects is on the order of tens of milliseconds. These fields can then add with other active dendrites and dendrite bundles to produce phase shifts that are detectable at the surface of the skull with MEG.

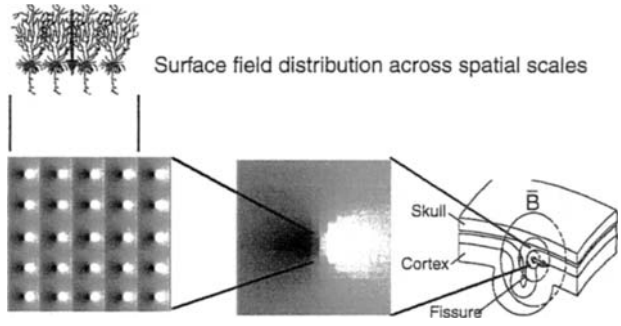

Fig. 7. Illustration of the multiple spatial scales of neuronal current-induced magnetic field shifts – from the surface field distribution from single dendrites to the field detected at the surface of the skull with MEG [8]. The map on the lower left is on the scale of tens of micrometers, showing the spatial distribution of the surface fields around dendrites These microscopic magnetic field changes cause spin-dephasing or magnitude changes. These dendrite surface potentials carry a net current that produces a larger scale dipole, shown on the middle map. This spatial scale is on the order of millimeters. Depending on the scale of the magnetic field inhomogenities, either a phase dispersion will take place as spins destructively add or a phase shift will take place (larger scale) as only a part of the magnetic field produced by the dipole is sampled by any one voxel. This dipole is what also hypothetically produces a net field distribution on the surface of the skull that is detectable by MEG.

of dendrite bundles is firing in a synchronized manner, there will be a distribution of microscopic surface potentials (as illustrated in Fig. 7) around each dendrite bundle. In addition, these bundles will form a cable which will manifest as a larger cylindrical (approximately) conductor that has a spatial dimension on the order of millimeters or even centimeters. This is the dipole source that has been simulated with phantoms. This is also a necessary manifestation of neuronal activity to produce a MEG-detectable signal. An important reminder is that the additive effect of neuronal bundles is not necessarily a cable or a single dipole but rather an amorphous distribution following proximal or distal cortical surfaces. As of yet, there has been no simulation of this effect that the authors of this article are aware of.

The study by Xiong et al. [7] also argued that BOLD contrast effects were minimized due to the rapid duty cycle (2 s interstimulus interval time) of the paradigm causing the BOLD contrast response to be saturated in the "on" state. It is intuitively clear that, given an absolutely constant interstimulus interval, the BOLD contrast effect would be nearly nonexistent. Nevertheless, if there is any jitter in the timing of the stimulus, it is possible that relatively slow hemodynamic responses may appear as ripples in the time course. This effect is illustrated in Fig. 8. In this simulation, the hemodynamic impulse response function [25] is convolved with a 200 ms duration stimulus that is repeated for 100 s

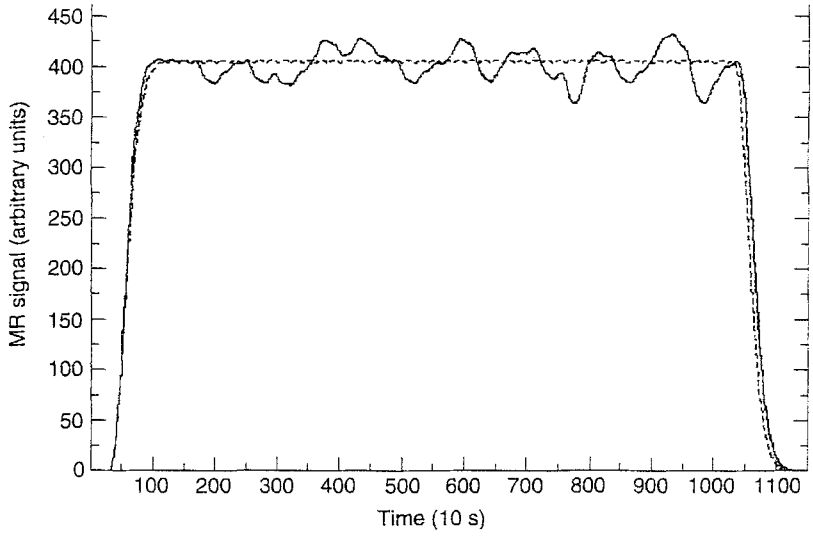

Fig. 8. Plot showing the simulated effects of BOLD contrast on top of the steady-state effect when activation timing is jittered with a timing on the order of that of reaction time variations. In this simulation, the hemodynamic impulse response function, according to ref. 25 is convolved with a 200 ms duration stimulus that is repeated for 100 s with a constant interstimulus interval of 2 s (dashed line) and an interstimulus interval that is varied between 2 ± 0.2 s (solid line). A 200 ms jitter was chosen to simulate a realistic range of reaction times. A randomly varying BOLD response having an amplitude of about 1/5 of the steady-state BOLD signal is present.

with a constant interstimulus interval of 2 s (dashed line) and an interstimulus interval that is varied between 2±0.2 s (solid line). A 200 ms jitter was chosen to simulate a realistic range of reaction times. A randomly varying BOLD response having an amplitude of about 1/5 of the steady-state BOLD signal is present. While the likelihood of this being the cause of this effect in this study is minimal, since the BOLD effect is random and the observed effect was a time-locked average, it is noted that the visual stimuli, having less variability in timing than the motor response, did not illicit an msMRI response, while the variable motor response did.

Lastly, the point was made in the Xiong et al. paper that the timing of this effect is similar to that detected with MEG and faster than the occasionally observed "preundershoot" in fMRI [13, 26–28], suggesting that the origin is not an increase in metabolic rate but rather the more rapid neuronal current effects. Nevertheless, it remains unclear whether or not a saturated BOLD would display a high-frequency component. Oscillations in oxygen consumption may represent a fast component of the BOLD response. Water molecules diffuse over a length on the order of tens of micrometers in tens of microseconds, which is close to the typical distance between capillaries. This means that the characteristic time of BOLD signal change associated with metabolic changes (oxygen being extracted from the blood rather than flow induced oxygenation increases) may be on the order of 100 ms which is a timing similar to that observed. Overall, while the findings of Xiong et al. are intriguing, considerably more work needs to be done to establish not only the repeatability of the findings but also the source of the signal changes.

In 2004, a careful study by Chu et al. [29], aimed directly at the study by Xiong et al. [7], reported the absence of any rapid phase or magnitude changes while BOLD effects and MEG signal changes were detected with the identical paradigm with high statistical significance. While it is of course impossible to definitively prove the lack of an effect from negative findings, the authors conclude that the effect is likely to be at least an order of magnitude less than BOLD contrast effects.

Lastly, a recently published article related to ncMRI by Park et al. [30] demonstrated neuronal current-induced MRI magnitude increases up to 5% in dissected snail ganglia with standard multishot spin-echo imaging at 3 T. Changes in phase were not reported. Neuronal activity was increased by application of sodium-nitrosocystein. While other MR effects, including changes in diffusion coefficient, T_1, or T_2 effects, were not ruled out, the authors speculate that these observed signal changes were due to neuronal-activity-induced microscopic changes in magnetic field.

In the past few years, several abstracts worth mentioning, yet to be published as papers, have been presented at scientific meetings. These include preliminary ncMRI findings in humans, ncMRI method development, further experimental findings in phantoms, and in vitro studies.

In 2004, Kilner et al. [31] reported successfully detecting neuronal current-correlated NMR phase and magnitude changes with a clever technique that in-

volved driving the visual cortex with a 10 Hz alternating checkerboard in a continuous manner, therefore saturating BOLD in the "on" state and subsampling the waveform at the TR of 1100 ms. It has been shown that the visual cortex is driven primarily at 2-fold the alternating rate for alternating checkerboard [32] and at the flicker rate for a flickering "on" and "off" stimulus. A demonstration of the manner in which visual cortex MEG signal follows the alternating checkerboard is shown in Fig. 9 from an experiment performed at the NIH MEG facility (data courtesy Rasmus Birn and August Tuan, Unit on Functional Imaging Methods, NIMH). Note that the photodiode represents 2-fold the alternating frequency since the sensitive region covered multiple black and white regions of the checkerboard. The MEG signal clearly follows the checkerboard. The strategy itself is illustrated in Fig. 10. Every TR, an MR image samples the waveform at a different phase of the cycle. The result would be a detectable beat frequency. The NIH group has attempted this strategy without clear success yet, but the work of Kilner et al. [31] shows promising results. It is still possible that any modulation in neuronal activity due to eye position or attention for instance might cause subtle BOLD contrast ripples. Nevertheless, an advantage in this technique is that the expected beat frequency can be modulated and modeled, therefore minimizing the effects of random signal fluctuations.

Bianciardi et al. [33] have further developed the concept of using a spin-echo to amplify transient phase shifts and suppress slow phase shifts by the use

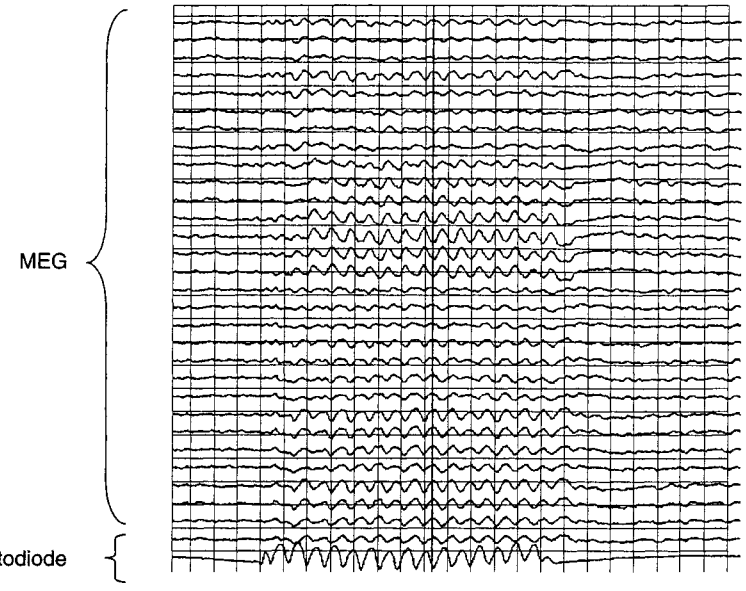

Fig. 9. MEG signal from sensors over the visual cortex. The stimulus was an 8 Hz alternating checkerboard. The photodiode measurement shows a frequency which is double the 8 Hz because the sensor covered a region that contained multiple black/white checkers. Note that the MEG signal follows the photodiode signal precisely. This type of stimulus is shown to illustrate the potential for having a precisely oscillating neuronal activity for the purposes of coordinating it with MRI acquisition timing.

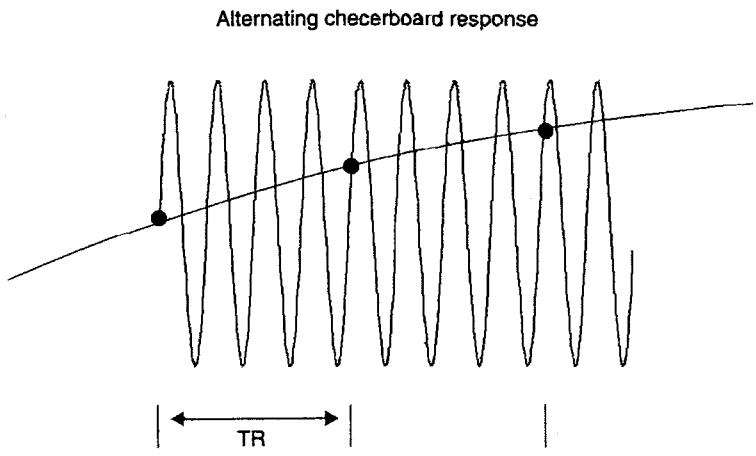

Fig. 10. Strategy for deriving ncMRI signal and avoiding BOLD. Here the visual system is driven in the manner shown in Fig. 8 for a long enough time to allow BOLD contrast to saturate in an elevated and hopefully steady state. Depending on the choice of TR relative to stimulus frequency, a beat frequency, created by the effect of oscillating neuronal currents, would be created and detectable by simple Fourier analysis, or by the use of a set of regressors in statistical parametric mapping (SPM) [29].

of a multiecho spin-echo sequence. They applied this to a simple neuronal current phantom with promising results. The goal here was simply to improve sensitivity, but one could also imagine adjusting the temporal gap between 180° pulses (typically known as τ) to selectively tune to specific neuronal frequencies.

Advantages of in vitro studies include a more tight control and measurement of the physiological environment. An in vitro study reported by Petridou et al. [34] is interesting because of the type of cell culture chosen and because of the high repeatability of the results. In this study, epileptic fetal rat brain cultures were imaged at 3 T in vitro, in active and inactive states. These tissue cultures were obtained from coronal sections of newborn-rat brains and contained cortical and basal ganglia tissue, which formed a feedback system exhibiting spontaneous and synchronized activity at less than 2 Hz [35]. Time series phase and magnitude images were collected on a 3 T GE scanner with single-shot spin-echo EPI (TE, 60 ms; TR, 1 s; slice thickness, 3 mm; matrix, 64 by 64 pixels; FOV, 18 cm). 300 images were collected per slice. Two data sets were acquired for each of the following states: active – spontaneous synchronized neuronal activity – and inactive – neuronal activity terminated by administering TTX (tetrodotoxin, a neuronal membrane sodium channel blocker). The power spectrum of the MRI phase time series was computed on a voxelwise basis. The findings reported in the abstract are shown in Fig. 11. On the bottom, right of the figure is a typical time series plot of the electrophysiologic recordings from these cultures. These demonstrate spontaneous bursting activity – a combination of low and high frequency behavior. The power spectrum shows distinct frequencies (A and B) that

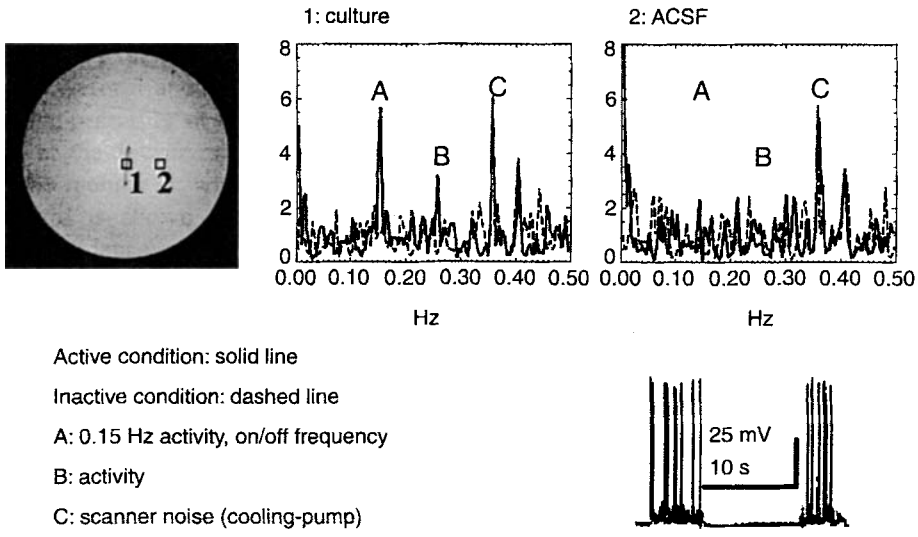

Fig. 11. Results from an in vitro study [34]. On the top left is a high-resolution MR image of a slide containing the fetal rat brain tissue culture. The slide is submerged in a ball of artificial cerebral spinal fluid (ACSF). On the bottom right is a typical time series plot of the electrophysiologic recordings from fetal rat brain cultures, showing spontaneous bursting activity – a combination of low and high frequency behavior – adopted from ref. 35. The two plots are the Fourier transforms of the time series MR phase from the cell culture (box on left in the image) and the ACSF (box on right in the image). The solid lines are from the culture when it is alive and spontaneously firing. The dotted lines are obtained approximately 20 min after administration of TTX, a sodium channel blocker, which essentially stops neuronal activity. The plots on the left show distinct frequencies (A and B) that disappear on administration of TTX. The plots on the right, from the ACSF, show no discernible change with administration of TTX. The higher frequency peak (C) is an artifact of the vibration caused by the cold head pump. These data were obtained using a GE 3 T scanner.

disappear on administration of TTX. The higher frequency peak (C) is an artifact of the vibration caused by the cold head pump of the scanner. The very-low-frequency peak is due to variable baseline drift. These results suggest that a non-BOLD contrast mechanism influences the MRI signal that influences NMR phase. Because it is unclear how changes in intrinsic T_1 and T_2 that may accompany neuronal firing could affect the NMR phase, these contrast mechanisms may be tentatively ruled out. Even though more work needs to be performed to rule out microscopic motion effects accompanying activity or cell swelling, this is a finding which provides potential evidence that biologically based neuronal currents are detectable at least in highly controlled systems.

Lastly, other abstracts that are of note include: detection of weak magnetic fields at 17.6 T using microscopy [36]; the use of simultaneously recorded electroencephalogram (EEG) and MRI to probe spontaneous and rapid changes in epileptic patients [37]; the use of simultaneous MEG and microtesla MRI towards detection of magnetic field changes [38]. It is emphasized that the combination of reduction of susceptibility noise, longer relaxation times, and no reduction in

the CURD contrast might make low-field imaging the technique of choice for ncMRI. Of course, lower SNR is problematic but potentially less problematic than ubiquitous BOLD effects if the utility of the technique grows. Lastly, at the date of completion of this manuscript, J. Prichard has reported collaborative success using a ncMRI technique that they call neurogenic inhomogeneity localization for detection of activity (J. Prichard et al., Brain Imaging Institute, Melbourne, Australia, pers. commun.).

3 Conclusion

Is neuronal current MRI a fantasy, possibility, or reality? It is heartening and exciting that neuronal current imaging efforts have been accelerating in the past five years. Steady progress in modeling, experimental design, pulse sequence specificity, processing, and sensitivity have clearly been made. Repeatable and convergent results in phantom studies and modeling efforts have been established. It has become evident that, without physiological noise, tightly controlled magnetic field changes on the order of 0.1 nT can be detected. Most models estimate that, at the spatial resolution of a voxel, this is about the magnitude of the field that is transiently produced by neuronal activity.

The primary problems in detection in humans are the an order of magnitude larger physiologic noise that is not readily filterable, the ubiquitousness of BOLD contrast – clouding the interpretation of results, the spatially variant and transient nature of neuronal activity, and the relatively small window (40 ms every second) that is available to investigators using EPI.

Areas where improvement should occur are in modeling, sensitivity, pulse sequence specificity, paradigm design, and processing. Modeling of neuronal activity at the intermediate spatial scale – between that of an individual axon and that of a magnetic field produced on the skull – is lacking. It is in work along this avenue where it seems that we will ultimately determine if neuronal current imaging is possible. Is there significant sub-dipole scale cancellation in neurogenic magnetic fields? At what scale is this cancellation at a maximum – centimeter, millimeter, micrometer? Can imaging at less than 3 mm^3 resolve this and therefore allow detection of current sources that are larger than estimated by skull surface values? How spatially variable are the dynamics? If one shifts the readout window, say, 50 ms, will the transient suddenly be detectable? These questions also need experimental trial and error where modeling falls short. With regard to sensitivity, higher field strengths and multichannel acquisition will likely allow higher resolution single-shot imaging (1 mm^3) and/or a factor of about 10 improvement in sensitivity in the next several years. This might make the difference, but we may still be an order of magnitude away in sensitivity. Nevertheless, pulse sequence development, allowing amplification of transient effects, show considerable promise. These also show promise in suppressing slow BOLD changes and artifactual changes resulting from cardiac and respiratory effects. Steady progress is being made towards modeling and therefore avoiding these artifactual signal changes. As we learn more about neuronal activity using other modalities we will

continue to design paradigms that allow us to tune our pulse sequences and processing methods to what specifically we are looking for. Simultaneous multimodal imaging will also help considerably in this approach. It may be that evidence for neuronal current-related changes is in the time series data that we currently have, and simply are waiting for the right processing method to decisively extract it.

Even though preliminary reports of success have been published, the lack of conclusive and reproducible results makes it difficult for anyone to claim that it is a reality. In conclusion, neuronal current imaging is solidly someplace between fantasy and reality – perhaps a bit more toward fantasy at this time. Even if it someday becomes a reality, its utility will likely at least initially be limited by the small size of the effect and the relatively small range of experiments possible using it due to the necessity for averaging or specific time-locked experiments. The progress in neuronal current MRI is already in stark contrast to that of fMRI using BOLD contrast, which arrived quite suddenly because the effect was extremely large and robust. It quickly became difficult to do an experiment and not see a result! By all measures, BOLD contrast-based fMRI (and perfusion contrast fMRI to a lesser degree) are increasing explosively in utility. It is impossible to predict breakthroughs, but this is precisely what neuronal current imaging needs to emerge as a technique that will allow us to ask even more insightful questions about how the human brain functions.

Appendix. Neuronal Activity

Structurally, a neuron is composed of three parts: the soma or cell body, a series of dendrites, and the axon. The soma is responsible for the synthesis of chemical components needed for the metabolic function of neuron, such as proteins, enzymes, and membrane components. Dendrites are intricate branching extensions from the soma that serve to receive information from other neurons via synapses. The synaptic site consists of a presynaptic element, which is usually the end segment of an axon, and a postsynaptic element located primarily on dendrites. The pre- and postsynaptic elements are separated by a 10 to 20 nm gap, termed synaptic cleft. The axon is a long cylindrical process extending from the soma and is responsible for information transfer from neuron to neuron. The majority of axons are covered by myelin, in segments of 0.2–2 mm, separated by a 1 mm gap (node of Ranvier). Myelin is formed by a lipid-type cell, the glial cell, which provides both electrical insulation and metabolic support to the neuron. Due to the lipid composition of myelin, axons appear white, unlike the soma and dendrites, thus the delineation of the brain into white and gray matter. Neurons vary from 5 to 100 mm in diameter, with soma and dendrite lengths ranging from 1.5 to 4.5 mm and axons ranging from 1 mm (e.g., interneurons) to 1 m or more (e.g., corticospinal tract).

Neurons are polarized cells. Their polarity arises by ion concentration differences between the intra- and extracellular fluids. Those differences are mainly

due to the higher concentration of sodium (Na^+), chloride (Cl^-), and calcium (Ca^{2+}) in the extracellular fluid and to the higher but unbalanced concentration of potassium (K^+) in the intracellular fluid. The resulting potential inside the neuron, the resting potential, is at approximately -65 mV and it is maintained by the unique properties of the neuronal membrane. The neuronal membrane consists of a 5–10 nm thick sheet of polarized phospholipids that is impermeable to ions, thus it acts as a capacitor preserving the neuron potential. The membrane is also infiltrated with ion channels (protein molecules) that allow the passage of ions in and out of the cell. Under resting conditions only a small number of ion channels are open, hindering ionic exchange between the intra- and extracellular fluids and maintaining the neuron resting potential. Ion channels thus act as resistors. Opening of ion channels is induced either by changes in membrane potential or chemical reactions during activation. The respective groups of channels are termed voltage-gated and ligand-gated. The best-described voltage-gated channels are the voltage-gated Na^+ and K^+ channels, which play a critical role in the action potential, and the voltage-gated Ca^{2+} channel, critical to presynaptic depolarization and synaptic activity. Prominent in the family of ligand-gated channels are postsynaptic receptors that enable ionic flow upon binding to a given neurotransmitter. In general, ion channels can be selective to a given ion, depending on their diameter and the size of the ion, and their distribution across the membrane dictates the electrical propagation of signals. The electrical properties of the neuronal membrane (capacitance, resistance, conductance) are referred to as the cable properties of neurons.

The neuronal membrane also contains ion pumps, a different group of protein molecules, that also assist in preserving the resting potential. An example of an ion pump is the Na^+/K^+ pump, which moves Na^+ ions out of the cell and K^+ into the cell. Pump activity is dependent on ionic concentration, i.e., the higher the ionic imbalance with respect to equilibrium, as in the case of an action potential, the faster the pump activity.

Electrical signaling by neurons is achieved by changes in the permeability of ion channels. Therefore, neuronal currents are carried by ions crossing the cell membrane due to the difference of ion concentration and potential between the intra- and extracellular fluids. Two types of electrical activity can be discriminated: the action potential and the synaptic potential. Information transfer from one neuron to another requires a synaptic potential to exist in both the pre- and postsynaptic elements, hence there are two types of synaptic potential: the presynaptic potential and the postsynaptic potential. Even though both pre- and postsynaptic potentials involve a change in ion channel permeability, the two processes are different.

The presynaptic element is characterized by a multitude of voltage-gated calcium channels and a multitude of vesicles containing neurotransmitter. Presynaptic vesicles are generally categorized according to size. Smaller ones (about 40 nm) consist of the majority of synaptic vesicles and are functionally connected to calcium channels, located very near the presynaptic membrane. The postsynaptic element on the other hand is characterized by a multitude of ligand-gated ion channels that bind

to the neurotransmitters released from the presynaptic elements. The ion selectivity of ligand-gated channels dictates the response at the postsynaptic site. Neurotransmitters that excite Na^+ ligand-gated channels, such as glutamate, will result in a depolarization of the membrane and an excitatory postsynaptic potential (EPSP). Neurotransmitters that excite Cl^- ligand-gated channels, such as GABA, will result in a hyperpolarization of the membrane and an inhibitory postsynaptic potential (IPSP). EPSPs increase the chance of the postsynaptic neuron firing an action potential and the propagation of information, while IPSPs decrease the chance of the postsynaptic neuron firing. The mechanism underlying both EPSP and IPSP is similar, therefore. The following discussion focuses on EPSP.

Depolarization at the presynaptic site of an active neuron, due to an action potential, will cause voltage-gated Ca^{2+} channels to open, resulting in an increase of intracellular Ca^{2+} concentration for 1–2 ms before Ca^{2+} either diffuses or is expelled by the Ca^{2+} pump. Within a few microseconds of depolarization, vesicles associated with the calcium channels release their neurotransmitter content in the synaptic cleft. Neurotransmitter binds to ligand-gated Na^+ channels at the postsynaptic site, resulting in local depolarization due to the local inflow of Na^+. The temporal extent of a single occurrence of the above events, at a single synapsis (about 1 μm in size), is a few milliseconds (an ion channel is open for 1–2 ms, and synaptic delay is approximately 1 ms) and the voltage change is less than 1 mV. For multiple synapses (order of hundreds to thousands per neuron) the summation of those events in space and time – termed temporal and spatial summation – yields the EPSP, which lasts 10 ms (single neuron) to 100 ms and is in the order of tenths of microvolts.

Once the postsynaptic site has depolarized by approximately 20 mV (−45 mV), an action potential is initiated at the neuronal axon. Action potentials propagate electrotonically in myelinated sections of the axon and actively in the nodes of Ranvier (saltatory conduction), as follows: within a few microseconds of an EPSP, axonal voltage-gated Na^+ channels open, allowing a rapid influx of Na^+ forcing the axonal membrane to depolarize, reaching a positive potential of approximately +20 mV within 0.5 ms. Depolarization triggers voltage-gated K^+ channels to open allowing a K^+ outflux, which forces the membrane potential to return to the resting state within 1 ms. Thus, the duration of an action potential is approximately 1 ms. Na^+ channels open and close within about 1 ms, while K^+ channels require 1–2 ms, resulting in an after-hyperpolarization of a few milliseconds ($\geq$2 ms). During the initial 1 ms, termed absolute refractory period, no further action potential can be initiated. During the following 1–2 ms, termed relative refractory period, an action potential can be initiated but would require a stronger EPSP. The two refractory periods translate into a maximum frequency for action potentials of 1 kHz. Furthermore, the refractory periods, coupled with the difference in anatomical and functional characteristics between the pre- and postsynaptic sites, ensure that electrical signals travel only in one direction.

References

1. Heeger D.J., Ress D.: Nat. Rev. Neurosci. **3**, 142–151 (2002)
2. Menon R.S., Kim S.G.: Trends Cogn. Sci. **3**, 207–216 (1999)
3. Ogawa S., Lee T.M., Kay A.R., Tank D.W.: Proc. Natl. Acad. Sci. USA **87**, 9868–9872 (1990)
4. Bandettini P.A. in: Functional MRI (Moonen C.T.W., Bandettini P.A., eds.), pp. 205–220. Berlin: Springer 1999.
5. Bodurka J., Bandettini P.A.: Magn. Reson. Med. **47**, 1052–1058 (2002)
6. Konn D., Gowland P., Bowtell R.: Magn. Reson. Med. **50**, 40–49 (2003)
7. Xiong J., Fox P.T., Gao J.-H.: Hum. Brain Mapp. **20**, 41–49 (2003)
8. Wikswo J., Vanegeraat J.: J. Clin. Exp. Neurophysiol. **8**, 170–188 (1991)
9. Song A.W., Takahashi A.M.: Magn. Reson. Imaging **19**, 763–767 (2001)
10. Darquie A., Poline J.-B., Poupon C., Saint-Jalmes H., Le Bihan D.: Proc. Natl. Acad. Sci. USA **98**, 9391–9395 (2001)
11. Prichard J., Zhong J., Petroff O., Gore J.: NMR Biomed. **8**, 359–364 (1995)
12. Janz C., Speck O., Hennig J.: NMR Biomed. **10**, 222–229 (1997)
13. Hennig J., Janz C., Speck O., Ernst T.: Int. J. Imaging Syst. Technol. **6**, 203–208 (1995)
14. Yablonskiy D.A., Ackerman J.H., Raichle M.E.: Proc. Natl. Acad. Sci. USA **97**, 9819–9819 (2000)
15. Yablonskiy D.A., Ackerman J.H., Raichle M.E.: Proc. Natl. Acad. Sci. USA **97**, 7603–7608 (2000)
16. Joy M., Scott G., Henkelman R.: Magn. Reson. Imaging **7**, 89–94 (1989)
17. Scott G., Joy M., Armstrong R., Henkelman R.: Magn. Reson. Med. **28**, 186–201 (1992)
18. Singh M.: IEEE Trans. Nuclear Sci. **41**, 349–351 (1994)
19. Bodurka J., Jesmanowicz A., Hyde J., Xu H., Estowski L., Li S.-J.: J. Magn. Reson. **137**, 265–271 (1999)
20. Kamei H., Iramina J., Yoshikawa K., Ueno S.: IEEE Trans. Magnetics **35**, 4109–4111 (1999)
21. Hatada T., Sekino M., Ueno S. in: Proceedings of the 12th Scientific Meeting of the International Society for Magnetic Resonance in Medicine, May 12–21, 2004, Kyoto, Japan (Duerk J.Z., ed.), p. 2222. Kyoto: ISMRM 2004.
22. Sekino M., Matsumoto T., Yamaguchi K., Iriguchi N., Ueno S.: IEEE Trans. Magnetics **40**, 1–3 (2004)
23. Song A.W., Li T. in: Proceedings of the 12th Scientific Meeting of the International Society for Magnetic Resonance in Medicine, May 12–21, 2004, Kyoto, Japan (Duerk J.L., ed.), p. 1063. Kyoto: ISMRM 2004.
24. Yamaguchi K., Sekino M., Ueno S., Iriguchi N.: J. Appl. Phys. **93**, 6739–6741 (2003)
25. Cohen M.S.: NeuroImage **6**, 93–103 (1997)
26. Hu X., Le T.H., Uğurbil K.: Magn. Reson. Med. **37**, 877–884 (1997)
27. Duong T.Q., Kim D.S., Uğurbil K., Kim S.G.: Magn. Reson. Med. **44**, 231–242 (2000)
28. Yacoub E., Shmuel A., Pfeuffer J., van de Moortele P.F., Adriany G., Uğurbil K., Hu X.P.: NMR Biomed. **14**, 408–412 (2001)
29. Chu R., de Zwart J.A., van Gelderen P., Fukunaga M., Kellman P., Holroyd T., Duyn J.H.: NeuroImage **23**, 1059–1067 (2004)
30. Park T.S., Lee S.Y., Park J.-H., Lee S.Y.: Neuroreport **15**, 2783–2786 (2004)
31. Kilner J.A., Stephan K.E., Josephs O., Friston K.J. in: Proceedings of the 10th International Conference on Functional Mapping of the Human Brain, Budapest, June 13–17, 2004, p. TH299, 2004.
32. Fawcett I.P., Barnes G.R., Hillebrand A., Singh K.D.: NeuroImage **21**, 1542–1553 (2004)
33. Bianciardi M., Cerasa A., Maraviglia B., Hagberg G.E. in: Proceedings of the 10th International Conference on Functional Mapping of the Human Brain, Budapest, June 13–17, 2004, p. TH299, 2004.
34. Petridou N., Bodurka J., Plenz D., Bandettini P.A. in: Proceedings of the 11th Scientific Meeting of the International Society for Magnetic Resonance in Medicine, July 1–16, 2003, Toronto, Ontario, Canada (Lomas D.J., ed.), Toronto: ISMRM 2003.
35. Plenz D., Kital S.T.: Nature **400**, 677–682 (1999)
36. Gulani V., Purea A., Schmitt P., Griswold M.A., Webb A.G. in: Proceedings of the 12th Scientific Meeting of the International Society for Magnetic Resonance in Medicine, May 12–21, 2004, Kyoto, Japan (Duerk J.L., ed.), p. 2314. Kyoto: ISMRM 2004.

37. Liston A., Salek-Haddadi A., Kiebel S., Turner R., Hamandi K., Lemieux L. in: Proceedings of the 10th International Conference on Functional Mapping of the Human Brain, Budapest, June 13–17, 2004, p. WE366, 2004.
38. Matlachov A.N., Volegov P., Espy M.A., Kraus R.H.J., George J.S. in: Proceedings of the 10th International Conference on Functional Mapping of the Human Brain, Budapest, June 13–17, 2004, p. WE366, 2004.

Authors' address: Peter A. Bandettini, Unit on Functional Imaging Methods, Functional MRI Facility, National Institute of Mental Health, Building 10, Room 1D80, 10 Center, Dr. MSC 1148, Bethesda, MD 20892-1148, USA
E-mail: bandettini@nih.gov